

Magnetic ordering, spin waves, and Haldane-gap excitations in $(\text{Nd}_x\text{Y}_{1-x})_2\text{BaNiO}_5$ linear-chain mixed-spin antiferromagnets

T. Yokoo,* S. Raymond,† A. Zheludev, and S. Maslov
Physics Department, Brookhaven National Laboratory, Upton, New York 11973

E. Ressouche
DRFMC/SPSMS/MDN Centre d'Etudes Nucleaires, 17 rue des Martyrs, 38054 Grenoble Cedex, France

I. Zaliznyak‡ and R. Erwin
NIST Center for Neutron Research, National Institute of Standards and Technology, Maryland 20899

M. Nakamura and J. Akimitsu
Department of Physics, Aoyama-Gakuin University, 6-16-1, Chitosedai, Setagaya-ku Tokyo 157 Japan
 (Received 4 March 1998)

Linear-chain nickelates with the composition $(\text{Nd}_x\text{Y}_{1-x})_2\text{BaNiO}_5$ ($x=1$, $x=0.75$, $x=0.5$, and $x=0.25$) are studied in a series of neutron-scattering experiments. Powder diffraction is used to determine the temperature dependence of the magnetic structure in all four systems. Single-crystal inelastic neutron scattering is employed to investigate the temperature dependence of the Haldane-gap excitations and low-energy spin waves in the $x=1$ compound $\text{Nd}_2\text{BaNiO}_5$. The results of these experiments are discussed in the context of the ‘‘Haldane chain in a staggered field’’ model for $R_2\text{BaNiO}_5$ systems, and quantitative agreement with theory is obtained. [S0163-1829(98)07945-4]

I. INTRODUCTION

The quantum-disordered ground state and the famous Haldane energy gap in the magnetic excitation spectrum¹ have kept one-dimensional (1D) Heisenberg antiferromagnets (AF's) at the center of attention of condensed-matter physicists for the last 15 years. Among the more recent developments are studies of such systems in external magnetic fields.²⁻⁵ It was found that in sufficiently strong fields one of the three Haldane-gap modes undergoes a complete softening. The result is a transition to a new phase with long-range antiferromagnetic correlations.^{6,7} The effect of a *staggered* field \mathbf{H}_π , to which a Haldane spin chain is most susceptible, is expected to be no less dramatic. Unfortunately, this problem has been given much less attention in literature, simply because such conditions are almost impossible to realize in an experiment. An *arbitrarily small* staggered field will induce a nonzero staggered magnetization in the Haldane chain. An intriguing question is how this induced order will affect the triplet gap excitations. Until recently the only 1D integer-spin AF's whose behavior was described in terms of a ‘‘staggered field’’ is $\text{Ni}(\text{C}_2\text{M}_8\text{N}_2)_2\text{NO}_2\text{ClO}_4$ (NENP), one of the best-known Haldane-gap materials [Refs. 8, 9, and references therein]. Due to the existence of two nonequivalent Ni sites in each chain, a weak effective staggered field is induced in NENP by a *uniform* external field.^{10,11} While the main effect on the spin dynamics is that of the uniform field, the staggered component produces a small yet observable effect.^{11,12}

The recent discovery of coexistence of Haldane-gap excitations and long-range magnetic order in $R_2\text{BaNiO}_5$ (R = magnetic rare earth) compounds¹³⁻¹⁵ presents a unique opportunity to investigate the effect of a staggered field experi-

mentally without having it obscured by the response of the system to a uniform component. According to our current understanding of the $R_2\text{BaNiO}_5$'s, long-range magnetic ordering does not destroy the quantum-disordered ground state of individual $S=1$ Ni chains in these quasi-1D systems. It is therefore essential that the Ni^{2+} ions carry an *integer*, as opposed to half-integer spin, and qualitatively different behavior is expected for isostructural half-integer spin materials like $\text{Nd}_2\text{BaCoO}_5$.^{16,17} The nonzero staggered magnetization that appears on the intrinsically disordered $S=1$ Ni chains below the Néel temperature T_N is viewed as being *induced* by an effective staggered exchange field generated by the ordered R sublattice.^{13,18} This physical picture will be referred to as the ‘‘Haldane chain in a staggered field’’ (HC/SF) model for $R_2\text{BaNiO}_5$ compounds.

In the HC/SF model, even in the magnetically ordered state, much of the dynamic spin correlations are contained in Haldane-gap modes propagating on the Ni chains. Below T_N these excitations coexist with low-energy order-parameter excitations, i.e., conventional spin waves, that involve correlated fluctuations of both Ni and rare-earth moments. The experimental confirmation of this was obtained in inelastic neutron-scattering experiments on $\text{Pr}_2\text{BaNiO}_5$,¹³ where Haldane-gap modes were clearly seen *both above and below the Néel temperature*. At all temperatures these excitations have a purely one-dimensional dynamic structure factor, and show no sign of softening at the 3D AF zone center at $T = T_N$. $\text{Pr}_2\text{BaNiO}_5$ samples are extremely difficult to prepare, and their magnetic properties are not always reproducible. For example, while magnetic ordering at $T_N=24$ K has been clearly observed in single crystals,¹³ for reasons yet unclear, no magnetic transition was observed in powders.¹⁹ It turned out that Nd-based linear-chain nickelates with the

general formula $(\text{Nd}_x\text{Y}_{1-x})_2\text{BaNiO}_5$ are more practical as model systems for neutron studies. On one side of this series ($x=0$) is Y_2BaNiO_5 , a well-studied Haldane-gap $S=1$ antiferromagnet with a spin gap $\Delta \approx 9$ meV.^{20–24} Y_2BaNiO_5 remains magnetically disordered even at low temperatures. At the other end we have $\text{Nd}_2\text{BaNiO}_5$ ($x=1$) that, thanks to the presence of magnetic Nd^{3+} ions, orders antiferromagnetically at $T_N=48$ K. As in the case of $\text{Pr}_2\text{BaNiO}_5$, Haldane-gap modes in $\text{Nd}_2\text{BaNiO}_5$ were found to survive in the magnetically ordered phase.¹⁴ Similar behavior was seen in $x=0.75$, $x=0.5$, and $x=0.25$ species, where the ordering temperatures are 39, 30, and 19 K, respectively.¹⁵ For all Nd concentrations at $T > T_N$ the Haldane-gap modes are virtually indistinguishable from those seen in Y_2BaNiO_5 . As the temperature is decreased through T_N , however, the gap energy Δ increases roughly linearly with $T_N - T$. This remarkable behavior is in agreement with theoretical predictions based on the HC/SF model.^{18,25}

To date, all inelastic measurements on $(\text{Nd}_x\text{Y}_{1-x})_2\text{BaNiO}_5$ materials were performed on powder samples. The existing magnetic structure (diffraction) data are not accurate or not complete enough to be discussed in relation to our model. Indeed, previous single-crystal experiments on the Nd system^{26,27} were analyzed assuming that the Nd and Ni moments are collinear at all temperatures below T_N . It was later shown that the actual structure is canted,²⁸ but no detailed temperature dependences derived from the canted model were reported. For the mixed Nd-Y systems only very preliminary results obtained by analyzing only three magnetic reflections are available.¹⁵

In this work we continue our studies of $(\text{Nd}_x\text{Y}_{1-x})_2\text{BaNiO}_5$ compounds using both elastic and inelastic neutron scattering. Powder neutron diffraction is used to investigate the temperature evolution of the magnetic structure in four $(\text{Nd}_x\text{Y}_{1-x})_2\text{BaNiO}_5$ species with $x=1$, $x=0.75$, $x=0.5$, and $x=0.25$, respectively. Inelastic neutron scattering is then employed to study the temperature dependence of the Haldane-gap excitations in the Ni-chains as well as the low-energy order-parameter fluctuations (spin waves) in single-crystal $\text{Nd}_2\text{BaNiO}_5$ samples. The connection between static and dynamic properties is discussed in the framework of the HC/SF model. Some of the results presented below were briefly discussed in Ref. 29.

II. EXPERIMENTAL PROCEDURES

The crystal structure of $R_2\text{BaNiO}_5$ compounds is discussed in great detail elsewhere.³⁰ All $(\text{Nd}_x\text{Y}_{1-x})_2\text{BaNiO}_5$ systems crystallize in an orthorhombic unit cell, space group $Immm$, $a \approx 3.8$ Å, $b \approx 5.8$ Å, and $c \approx 11.7$ Å.¹⁵ The $S=1$ Ni chains are formed by orthorhombically distorted NiO_6 octahedra that are lined up in the $[100]$ crystallographic direction, sharing their apical oxygen atoms. The R sites (occupied at random by Y or Nd) are positioned in between these chains. The site symmetry for the R^{3+} is low and the electronic ground state for Nd^{3+} is a Kramers doublet.

In powder-diffraction experiments on the $x=0.75$, $x=0.5$, and $x=0.25$ compounds we used the same samples (roughly 15 g each) as in previous inelastic studies.¹⁵ A new $\text{Nd}_2\text{BaNiO}_5$ ($x=1$) powder sample of comparable mass was prepared particularly for the present study using the

solid-state reaction method. Powder neutron-diffraction experiments were carried out at the high flux reactor of the Institut Laue-Langevin (Grenoble), on the 400 cells position sensitive detector diffractometer D1B for the $x=0.75$, $x=0.5$, and $x=0.25$ compounds and on the 1600 cells diffractometer D20 for the $x=1$ system. The patterns were recorded in the temperature range 2–50 K, using a liquid-helium cryostat. The wavelengths $\lambda=2.526$ Å on D1B and $\lambda=2.400$ Å on D20 were provided in both cases by focusing pyrolytic graphite monochromators. The samples were enclosed in cylindrical vanadium containers. The analysis of the powder patterns was performed by Rietveld profile refinement using the software FULLPROF.³¹ A pseudo-Voigt function was chosen to generate the line shape of the diffraction peaks. The scattering lengths were taken from Ref. 32 and the magnetic form factors of Nd and Ni from Ref. 33.

Single-crystal samples for inelastic neutron-scattering experiments were grown in oxygen atmosphere using the floating-zone technique. Most of the thermal neutron inelastic measurements were done on a cylindrical single-crystal 25 mm long and 4 mm in diameter (sample A) with mosaic about 0.3° . Only near the end of this series of experiments did a much larger sample (sample B) become available. Sample B consists of three single crystals, each roughly 6 mm in diameter and 50 mm long with an $\approx 0.8^\circ$ mosaic. The three crystals were aligned together on a specially designed aluminum sample holder. The resulting “supersample” had a symmetric mosaic of around 1.2° . Sample B was used primarily in cold-neutron inelastic scattering experiments.

Inelastic thermal neutron-scattering measurements were carried out at the Center for Neutron Research at the National Institute of Standards and Technology (NIST) on the BT-4 and BT-2 triple-axis spectrometers. The samples were in all cases mounted with the $(h,0,l)$ reciprocal-space plane parallel to the scattering plane of the spectrometer. A neutron beam of 14.7 meV fixed final energy was used with $60' - 40' - 40' - 120'$ collimations and a pyrolytic graphite (PG) filter positioned after the sample. PG (002) reflections were used for monochromator and analyzer (setup I). The measurements were done with energy transfers up to 25 meV, the calculated resolution at a typical 15 meV energy transfer being 2.5 meV full width at half maximum (FWHM). The sample environment was a standard displax refrigerator, and measurements were done in the temperature range 25–60 K. As we have found, in all samples the axis of the cylindrical crystal roughly coincides with $[100]$ crystallographic direction. In the experiment the sample cylinder was therefore positioned horizontally in the scattering plane, which resulted in substantial absorption effects. The effective transmission coefficient as a function of sample orientation was determined by measuring the intensity of incoherent scattering. The measured absorption correction was almost constant within each constant- Q scan performed, but varied by as much as a factor of 2 between different Brillouin zones.

Inelastic cold neutron-scattering experiments were done on the SPINS three-axis spectrometer at NIST. Several configurations were used. In setup II we utilized $30' - 80' - 80' - \text{open}$ collimations with a 3.7 meV fixed final energy neutron beam and a BeO filter after the sample. In this setup the energy resolution at zero energy transfer is 0.2 meV FWHM. 5 meV fixed-final energy neutrons were used in

setup III with the same collimation setup and a Be filter positioned after the sample. A substantial gain in intensity (at the cost of wave vector resolution) was obtained using $30' - 80' - 45'$ (radial)–open collimations and 5.1 meV fixed final energy neutrons, a Be-filter after the sample and a horizontally focusing analyzer (setup IV). The energy resolution in this case was 0.35 meV FWHM at zero energy transfer. The sample environment was a displacer refrigerator and the temperature was controlled in the range 10–50 K.

III. EXPERIMENTAL RESULTS

A. Magnetic structure

For all samples studied the diffraction patterns in the paramagnetic phase were found to be totally consistent with the crystal structure reported in Ref. 30. A small amount of nonmagnetic impurities was detected in the $x=0.75$, $x=0.5$, and $x=0.25$ samples, whereas the $x=1$ one turned out to be single phase. The small extra peaks due to this impurity were excluded from the refinements.

As previously observed,¹⁵ magnetic ordering in all samples manifests itself in the appearance of new Bragg reflections at half-integer positions, the magnetic propagation vector being $[1/2 \ 0 \ 1/2]$. In the $x=1$ sample, thanks to the relatively strong magnetic signal, a simultaneous refinement of nuclear and magnetic structures could be performed. A typical powder scan for this system is shown in Fig. 1(a). For the other three compounds, where the magnetic signal was weaker, a different approach was used. For powder scans collected at $T < T_N$ the magnetic contribution to scattering was isolated by subtracting the nuclear background measured just above the ordering temperature. Several typical data sets obtained in this fashion are shown in Figs. 1(b)–1(d).

In the $x=0.25$ sample, in addition to the above-mentioned magnetic peaks at half-integer positions, extra intensity below T_N was also observed at the positions of nuclear peaks [Fig. 1(d)]. One possible explanation for this is the presence of an extra magnetic component in the structure of this compound. This, however, appears not to be the case. We were unable to reproduce the observed pattern with any reasonable spin model. In addition, the intensities of these extra reflections seem to *increase* with increasing scattering angle, strongly suggesting that they are of nuclear, rather than magnetic origin. In our analysis we have assumed that these extra peaks represent a lattice distortion that is induced by magnetic ordering. In the determination of the magnetic structure of this sample these reflections were therefore ignored.

According to the analysis of the crystallographic space group of $R_2\text{BaNiO}_5$ compounds ($Immm$), only two types of magnetic structure with propagation vector $[1/2 \ 0 \ 1/2]$ and nonzero magnetic moment on both Ni and R sites are possible.³⁴ In the structure realized in $\text{Er}_2\text{BaNiO}_5$ all spins are confined to the (a,b) crystallographic plane. As shown by several previous studies,^{26,28} it is the other alternative that is realized in $\text{Nd}_2\text{BaNiO}_5$: both the Ni^{2+} and Nd^{3+} moments are in the (a,c) plane of the crystal (Fig. 2). We used this model to fit the diffraction spectra measured at each temperature for each sample. The adjustable parameters were the magnetic moments $m^{(\text{Ni})}$ and $m^{(\text{Nd})}$ of the Ni^{2+} and Nd^{3+} ions, respectively, as well as the angles $\phi^{(\text{Ni})}$ and $\phi^{(\text{Nd})}$

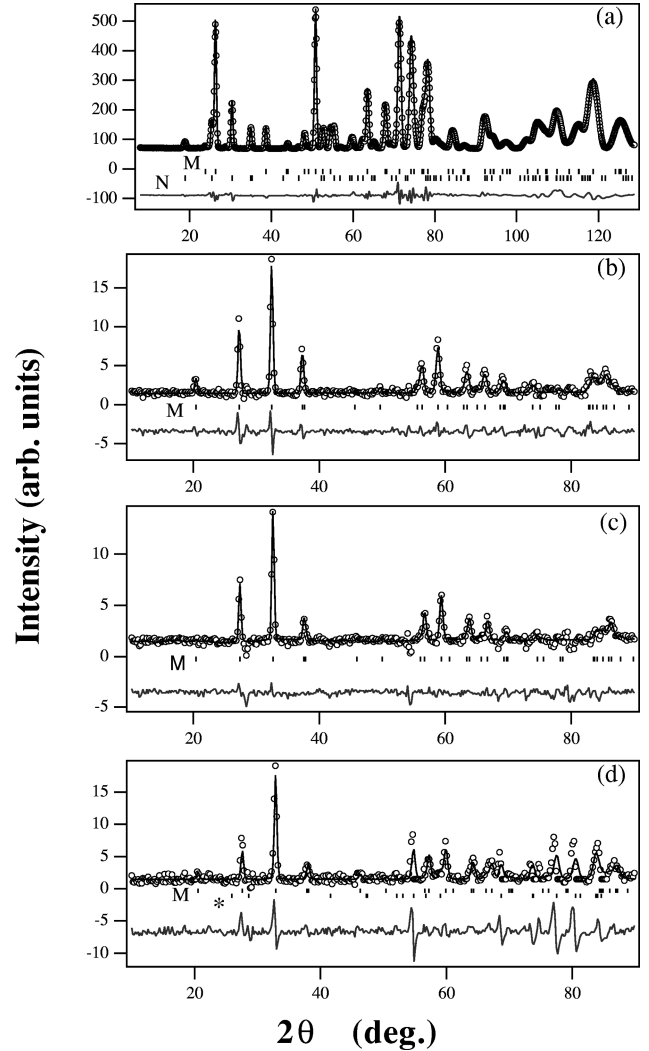


FIG. 1. Typical measured (symbols) and calculated (solid curve) powder-diffraction profiles for $(\text{Nd}_x\text{Y}_{1-x})_2\text{BaNiO}_5$ samples with $x=1$ (a), $x=0.75$ (b), $x=0.5$ (c), and $x=0.25$ (d), and the corresponding residuals (obs - calc). For $x=1$, the full diffraction pattern (nuclear and magnetic) is shown. For the three other compounds, the nonmagnetic scattering profile was measured just above the Néel temperatures and subtracted from shown scans. The ticks indicate the positions of Bragg reflections, both nuclear (N) (in the $x=1$ compound) and magnetic (M). In the magnetically ordered phase of the $x=0.25$ compound (d), additional intensity is also observed at nuclear Bragg peak positions (marked with an *).

these moments form with the c axis of the crystal. Good fits to the experimental powder profiles, examples of which are shown in solid curves in Fig. 1, were obtained in all cases. The refined values of parameters are plotted against temperature in Figs. 3 and 4. As observed in previous studies,²⁸ near the Néel temperature the magnetizations of both Ni and Nd sublattices undergo a slight reorientation with decreasing temperature. Very quickly though this reorientation slows down and in all samples the angles $\phi^{(\text{Ni})}$ and $\phi^{(\text{Nd})}$ remain at roughly -35° and 0° , respectively, in most of the temperature range.

B. Ni-chain gap excitations

The temperature dependencies of energies and intensities of the Haldane-gap excitations were studied by inelastic ther-

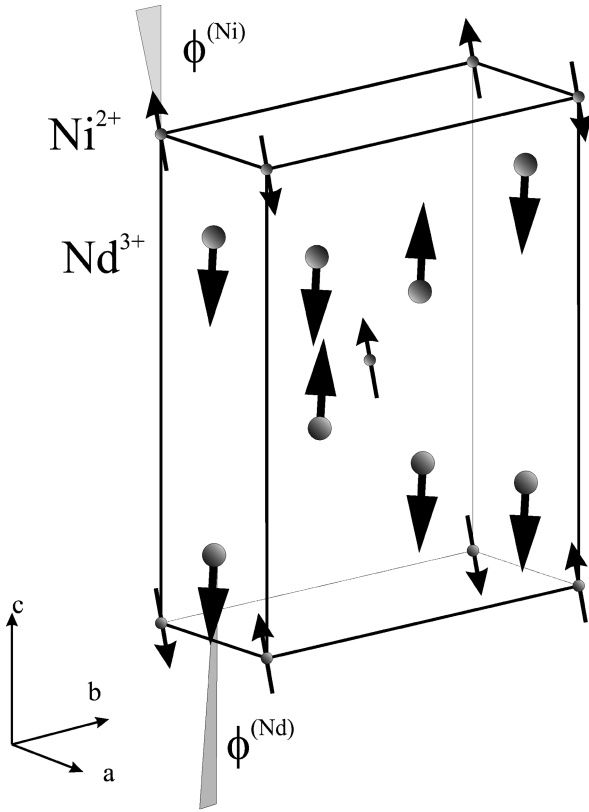


FIG. 2. A schematic view of the magnetic structure of $\text{Nd}_2\text{BaNiO}_5$. A single crystallographic unit cell is shown. The magnetic moments of both Ni^{2+} and Nd^{3+} are confined to the (a, c) crystallographic plane. The magnetic propagation vector is $[\frac{1}{2}0\frac{1}{2}]$.

mal neutron scattering. One of our objectives was to use the intrinsic polarization dependence of the neutron-scattering cross section to distinguish between the three individual modes, expected to be present in the Haldane multiplet. For this purpose the data were collected in constant- Q scans at the 1D antiferromagnetic zone centers $\mathbf{Q}=(1.5,0,0)$ and $\mathbf{Q}=(0.5,0,4.2)$. These wave vectors correspond to equal momentum transfers, but are pointing along and almost perpendicular to the Ni-chain axis a , respectively. At $(1.5,0,0)$ only the fluctuations of y and z spin components are seen (the axes x , y , and z are chosen along the $[100]$, $[010]$, and $[001]$ directions, respectively), while at $(0.5,0,4.2)$ it is mostly the fluctuations of x and y spin components that contribute to the scattering intensity.

The most serious obstacle in previous powder measurements was the presence of two crystal-field (CF) excitations associated with Nd^{3+} that appear at about 18 and 24 meV, respectively.¹⁴ Unlike the highly dispersive Haldane excitations, the dispersionless CF modes do not suffer an intensity penalty upon powder averaging the corresponding dynamic structure factors. The Haldane modes that appear at ≈ 10 meV energy transfer at $T=50$ K and move towards higher energies at lower temperature are thus very difficult to separate from the intense CF background. In a single crystal this problem may be overcome. First, the intensity of Haldane modes relative to those of CF excitations is much larger in this case. Second, in a single crystal the background can be directly measured at scattering vectors slightly off the 1D zone center, where the Haldane excitations move out of

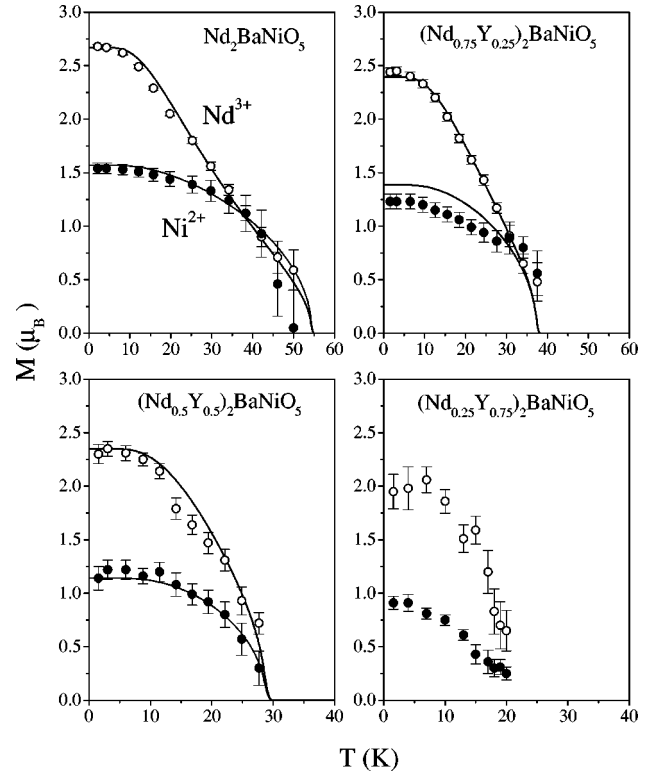


FIG. 3. Temperature dependence of the ordered moment on the Ni (solid circles) and Nd (open circles) sites in $(\text{Nd}_x\text{Y}_{1-x})_2\text{BaNiO}_5$ samples for $x=1$, $x=0.75$, $x=0.5$, and $x=0.25$. The data points (circles) are determined from profile refinement of experimental diffraction patterns (see Sec. III) and the solid curves are calculated from the mean-field model [Eqs. (4)–(8) in Sec. IV].

the scan range thanks to their steep dispersion. In our case the background was measured at $\mathbf{Q}=(1.4,0,0)$ and $\mathbf{Q}=(0.4,0,4.2)$. Since it was previously found that the CF modes are slightly temperature dependent, the background measurements were performed separately at each temperature. Figure 5 shows some typical data collected in sample A at $T=50$ K (open circles) together with the corresponding background scans (solid circles). The result of point-by-point subtraction is shown in Fig. 6. The well-defined peak at ≈ 11 meV energy transfer, very similar to that previously seen in Y_2BaNiO_5 (Refs. 20–24) and $\text{Pr}_2\text{BaNiO}_5$,¹³ is attributed to the Haldane excitations in the Ni chains.

One problem that had to be dealt with was the presence of a spurious peak at roughly 18 meV energy transfer (see Fig. 5). We have identified this spurious peak as being caused by higher-order scattering ($2k_i$) in the monochromator, incoherent and/or Bragg scattering in the sample, and higher-order ($3k_f$) scattering in the analyzer. In the analysis described below the “dangerous” energy range has been excluded from all data sets.

Ideally, for a complete determination of the mode polarization, at each temperature one would analyze the inelastic scans collected at both wave vectors simultaneously, using a model cross section that would include three modes with separate gap values and polarization factors. In the present study, however, as the structure of the observed peak is totally smeared by the broad instrumental resolution, using a three-component model cross section results in an over-

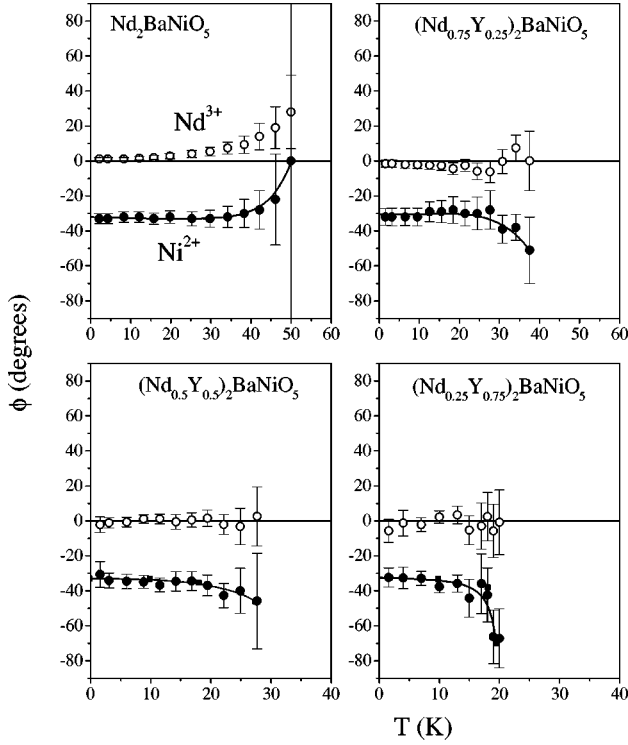


FIG. 4. Temperature dependence of the angle between the crystallographic c axis and the Ni (solid circles) and Nd (open circles) ordered moments in $(\text{Nd}_x\text{Y}_{1-x})_2\text{BaNiO}_5$ samples for $x=1$, $x=0.75$, $x=0.5$, and $x=0.25$. Solid curves are guides to the eye. The data points (circles) are determined from profile refinement of experimental diffraction patterns (see Sec. III).

parametrized problem. Instead we analyzed all the measured inelastic scans separately using a single-mode cross section, as was previously done for $\text{Pr}_2\text{BaNiO}_5$.¹³ The model dynamic structure factor was written in the “double-Lorentzian” form:

$$S(\tilde{q}, \omega) = \frac{S_0 \xi / \Gamma}{1 + \tilde{q}^2 \xi^2 + (\omega - \omega_{\tilde{q}})^2 / \Gamma^2}, \quad (1)$$

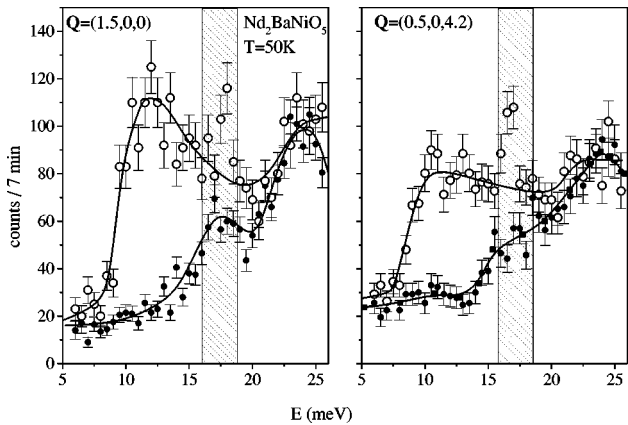


FIG. 5. Typical inelastic scans measured in single-crystal $\text{Nd}_2\text{BaNiO}_5$ (sample A) at the 1D antiferromagnetic zone centers (open symbols) and background scans taken slightly off these positions (solid symbols) at $T=50$ K. The shaded areas indicate the scan range contaminated by a $2k_i - 3k_f$ spurion. The solid curves are guides for the eye.

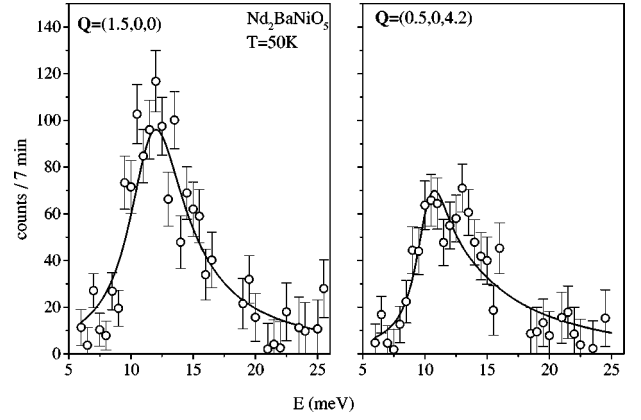


FIG. 6. Typical inelastic scans (background subtracted) measured in single-crystal $\text{Nd}_2\text{BaNiO}_5$ (sample A) at the 1D antiferromagnetic zone centers (open symbols). The solid curves are fits with a model cross section as described in Sec. IV [Eqs. (1) and (2)].

$$(\hbar \omega_{\tilde{q}})^2 = \Delta^2 + c^2 \tilde{q}^2. \quad (2)$$

In this formula \tilde{q} is the projection of the scattering vector \mathbf{q} onto the chain axis, and measured relative to the 1D antiferromagnetic zone center; Δ is the gap energy; c is the spin-wave velocity along the chains; Γ is the intrinsic energy width of the excitations; and ξ is the real-space dynamic spin-correlation length. Since all measurements were performed at $\tilde{q}=0$, the parameters ξ and c are only needed to properly take into account focusing effects. In our analysis ξ and c were therefore fixed to the values previously measured in $\text{Pr}_2\text{BaNiO}_5$: $1/\xi=0.08 \text{ \AA}^{-1}$, and $c=200 \text{ meV \AA}$. For each scan the cross section (1) was folded with the four-dimensional spectrometer resolution function and the parameters Δ , Γ and the prefactor S_0 were refined to best fit the data. To further minimize the number of independent variables we have averaged the value of Γ determined at different temperatures and used this average as a fixed parameter in the final fit. This was done separately for $\mathbf{Q}=(1.5,0,0)$ and $\mathbf{Q}=(0.5,0,4.2)$, where the average values were 2 and 1.5 meV, respectively. Several typical fits of Eqs. (1),(2) to our inelastic data are shown in solid curves Fig. 7. The obtained temperature dependences for Δ and S_0 for both wave vectors are shown in Fig. 8.

C. Low-energy spin waves

The main purpose of the cold-neutron experiments was to study the low-energy order-parameter fluctuations in $\text{Nd}_2\text{BaNiO}_5$. Usually, such excitations resulting from long-range ordering appear as acoustic spin waves, as previously observed in $\text{Pr}_2\text{BaNiO}_5$.¹³ For $\text{Nd}_2\text{BaNiO}_5$ most of the measurements were done in the vicinity of the $(0.5,0,1.5)$ magnetic Bragg reflection, one of the strongest magnetic peaks in the (a,c) plane, with roughly 10 000 counts per second at $T=10$ K using setup II. To search for the acoustic spin waves we used configurations I, II, or III to perform constant- Q scans at wave vectors $(0.5,0,1.5)$, $(0.75,0,1.5)$, $(1,0,1.5)$, and $(1.5,0,1.25)$ in the range 0–8 meV (Fig. 9), as well as constant- E scans at an energy transfer $\hbar\omega=0.3$ meV along $(0.5+\zeta,0,1.5)$ and $(0.5,0,1.5+\zeta)$ ($-\zeta=0.25$

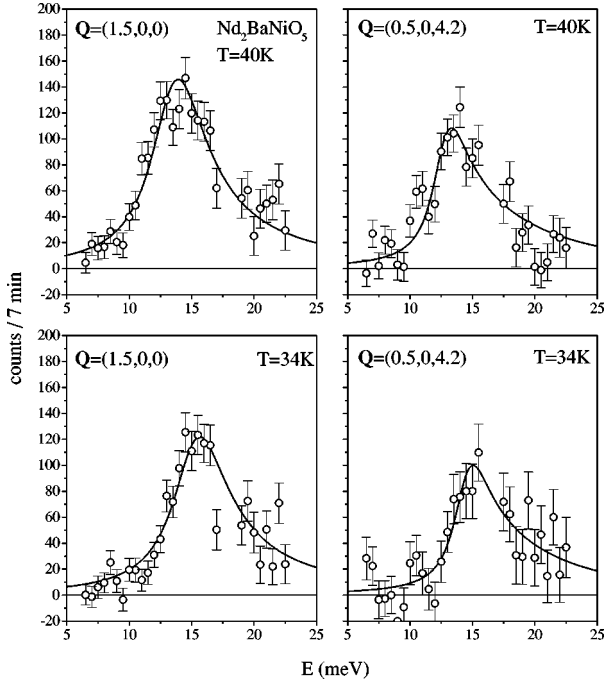


FIG. 7. Typical inelastic scans (background subtracted) measured in single-crystal $\text{Nd}_2\text{BaNiO}_5$ (sample B) at the 1D antiferromagnetic zone centers (open symbols) at several temperatures. The solid curves are fits with a model cross section as described in Sec. IV [Eqs. (1) and (2)].

$\lesssim \zeta \lesssim 0.25$). At $T = 10$ K absolutely no inelastic signal was found at energy transfers below ≈ 4 meV. At $\hbar\omega = 4$ meV we observe the rather intense resolution-limited inelastic feature previously seen in powder experiments.¹⁴ The 4 meV excitation is totally dispersionless along both the a and c axes of the crystal. This can be deduced from Fig. 10, that shows some typical constant- Q scans collected at several wave vectors at $T = 10$ K. Scanning through the 4 meV peak in different Brillouin zones led us to the conclusion that the mode is a single-ion excitation with no unit-cell structure factor and no apparent polarization dependence of intensity. The accessible range of momentum transfers was not sufficient for an accurate study of the form-factor dependence of the intensity.

What makes the 4 meV mode rather interesting is its temperature dependence. As was previously established in inelastic neutron-scattering experiments on powder samples,¹⁴ this excitation is visible only at $T < T_N$. As the Néel temperature is approached from below the excitation energy decreases, the width increases dramatically (Fig. 11), and at $T = T_N$ the mode appears to merge with quasielastic scattering at $\hbar\omega = 0$. We have utilized setups I and IV to measure the temperature dependence of the excitation energy for temperatures up to $T = 35$ K, where the inelastic peak is broad, yet still easily identified. Constant- Q scans were analyzed with a damped-oscillator dynamic structure factor:

$$S(\omega) = \frac{I_0 \gamma [n(\omega) + 1]}{\omega_0 \pi} \left[\frac{1}{(\omega - \omega_0)^2 + \gamma^2} - \frac{1}{(\omega + \omega_0)^2 + \gamma^2} \right], \quad (3)$$

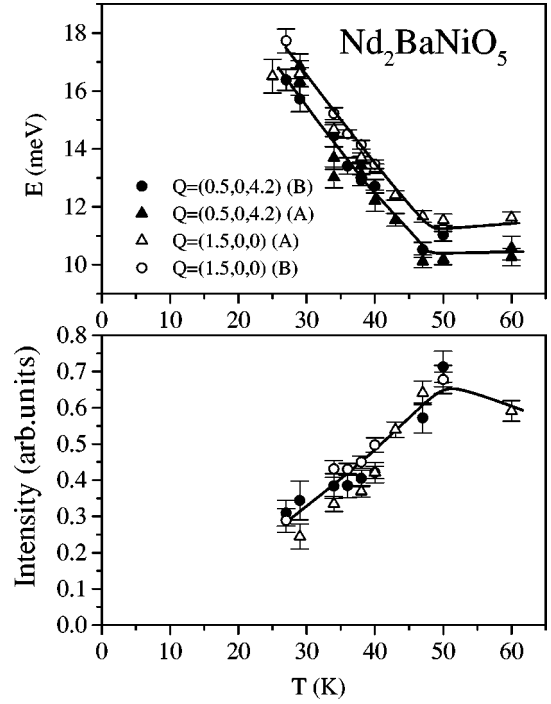


FIG. 8. Measured temperature dependences of the gap energy (top) and energy-integrated intensity (bottom) of Ni-chain Haldane excitations in single-crystal $\text{Nd}_2\text{BaNiO}_5$. Triangles and circles show data obtained in the two samples studied. The solid curves are guides to the eye.

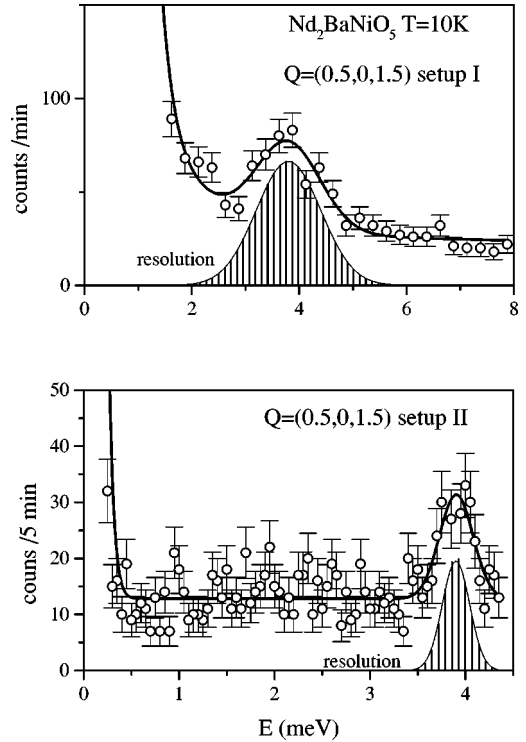


FIG. 9. Sample inelastic scans measured in $\text{Nd}_2\text{BaNiO}_5$ (sample B) at the magnetic Bragg position (0.5,0,1.5) using thermal (top) and cold (bottom) neutrons at $T = 10$ K. Apart from the resolution-limited feature at 4 meV energy transfer, no inelastic scattering is observed above background level up to 8 meV energy transfer. Solid curves are guides to the eye.

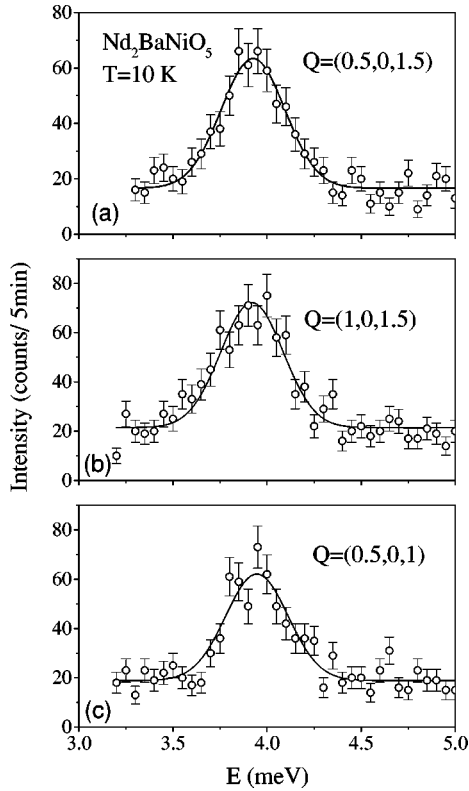


FIG. 10. Sample inelastic scans measured in $\text{Nd}_2\text{BaNiO}_5$ (sample B) at the magnetic Bragg zone center (a) and zone boundaries (b,c) illustrate the absence of any dispersion in the 4 meV excitation at $T=10$ K. Solid curves are Gaussian fits.

that was convoluted with the Gaussian energy resolution of the spectrometer (solid curves in Fig. 11). In Eq. (3) $n(\omega)$ is the Bose factor and I_0 is the structure factor of the excitation. For $\mathbf{Q}=(0.5,0,1.5)$ the experimental T dependences of the excitation energy $\hbar\omega_0$ and relaxation rate γ are shown in Fig. 12. The same behavior was also seen at $\mathbf{Q}=(0.75,0,1.5)$ and $\mathbf{Q}=(1,0,1.5)$.

IV. DISCUSSION

A. Magnetic ordering

In previous resonant magnetic x-ray-diffraction studies²⁷ it was found that the order-parameter critical exponent β in $\text{Nd}_2\text{BaNiO}_5$ is indistinguishable from the mean-field (MF) value $\beta=0.5$. In fact, for the $x=1$ system, the standard MF theory can accurately describe the entire temperature dependence of both Ni and Nd ordered moments.²⁷ In this model *both* Ni^{2+} and Nd^{3+} ions are treated as isolated spins in an effective exchange field, and their bare magnetization curves are given by appropriate Brillouin functions. The reduced moment on the Ni sites (the expected value is $2\mu_B$) is attributed to orbital effects (reduced g factor). Despite the fact that reasonably good fits to the experimental temperature dependences can be obtained by applying this simple approach to each $\text{Nd}_2\text{BaNiO}_5$ compound separately, the refined Ni-Nd and Ni-Ni coupling parameters, as well as the g factor for Ni^{2+} depend greatly upon sample composition. Such a strong variation of the Ni-Ni exchange constant is difficult to explain by the slight composition dependence of

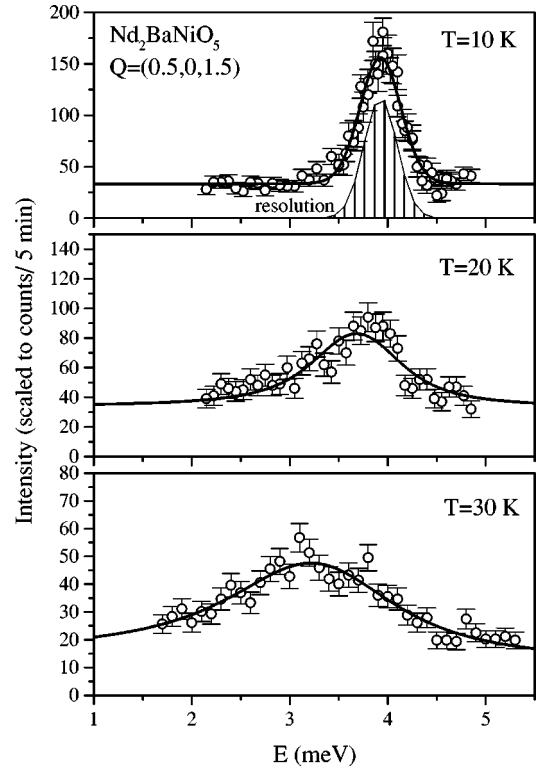


FIG. 11. Temperature evolution of the 4 meV excitation measured in $\text{Nd}_2\text{BaNiO}_5$ (sample B) at the magnetic Bragg position $(0.5,0,1.5)$. The solid curves represent empirical fits as described in Sec. IV (Eq. 3). At $T>T_N=48$ K the excitation is totally unobservable.

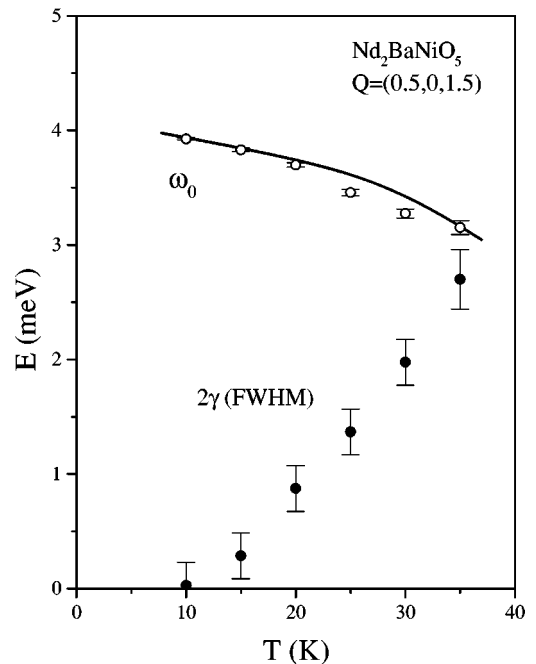


FIG. 12. Measured temperature dependence of the energy squared (open circles) and full energy width at half maximum (solid circles) of the 4 meV excitation in $\text{Nd}_2\text{BaNiO}_5$ (sample B). The solid curve is a theoretical curve as described in Sec. IV [Eq. (10)].

the lattice parameters and hence the Ni-Ni exchange integral.¹⁵ Indeed, the Haldane-gap energies in the paramagnetic phase are directly proportional to the Ni-Ni exchange constant, and were previously found to be independent of Nd content.¹⁵ If we are to describe the measured temperature dependences of sublattice magnetizations in $(\text{Nd}_x\text{Y}_{1-x})_2\text{BaNiO}_5$, treating magnetic interactions at the MF level, we have to look for a different approach.

In-chain Ni-Ni AF exchange coupling is by far the strongest magnetic interaction in $R_2\text{BaNiO}_5$ compounds ($J_{\text{Ni-Ni}} \approx 300$ K). At $T \leq \Delta$, which, incidentally is the temperature range where long-range magnetic ordering occurs, the susceptibility of the Ni subsystem is therefore dominated by well-established in-chain correlations. In this situation it is *not appropriate* to model the magnetic transition by treating the Ni^{2+} ions as isolated moments. Instead, the MF theory should treat entire Ni chains as inseparable entities, characterized by their bare staggered magnetization function. Three-dimensional long-range ordering is driven by the next important magnetic interaction, namely Ni-R exchange coupling that establishes links between individual chains and is of the order of tens of Kelvin. Direct R-R interactions are expected to be very weak (of the order of 1 K or less) and can for this reason be disregarded.¹⁹

Garcia-Matres *et al.*¹⁹ analyzed their magnetic susceptibility data treating only the Ni-R interactions at the MF level. The experimentally measured temperature dependence of the Ni-order parameter was built into this model as an empirical function. The HC/SF model provides a physical justification for this approach:²⁹ the bare magnetization curve for the Ni subsystem is to be taken in the form of the *staggered magnetization function for an isolated quantum-disordered Haldane chain*. This ‘‘semiquantum’’ model differs qualitatively from the standard MF model for classical magnets. In the latter, at $T \rightarrow 0$ all sublattices become fully saturated as the bare single-ion susceptibility diverges as $1/T$. In contrast, the bare staggered susceptibility χ_π of a Haldane spin chain remains *finite* at $T=0$, and the Ni sublattice need not be fully saturated. The ‘‘semiquantum’’ model can thus account for the reduced ordered moment on the Ni sites without assuming an improbably small g factor for Ni^{2+} . Moreover, it will predict qualitatively different temperature dependences, since the staggered susceptibility of a Haldane spin chain, unlike the single-ion susceptibility, is expected to be almost T independent at $T \leq \Delta$ ($\Delta \approx 9$ meV, or ≈ 105 K in $R_2\text{BaNiO}_5$ compounds).

It has to be noted that treating interchain coupling at the MF or RPA (random phase approximation) level is, in itself, not a new idea, but a well-established technique.³⁵ In their pioneering work on CsNiCl_3 , the first Haldane-gap material studied experimentally, Buyers *et al.*,³⁶ and Affleck³⁷ implemented this approach to explain magnetic ordering and calculate the spin-wave dispersion relations. The main difference between CsNiCl_3 and $R_2\text{BaNiO}_5$ is that exchange coupling between individual Haldane chains is *direct* in the former system, and *mediated by the rare-earth ions* in the latter. For directly coupled Haldane spin chains, the magnitude of interchain interactions must exceed some critical value in order for the system to order magnetically.³⁷ In a MF description of CsNiCl_3 or any other system with directly coupled quantum chains, the temperature dependence of the

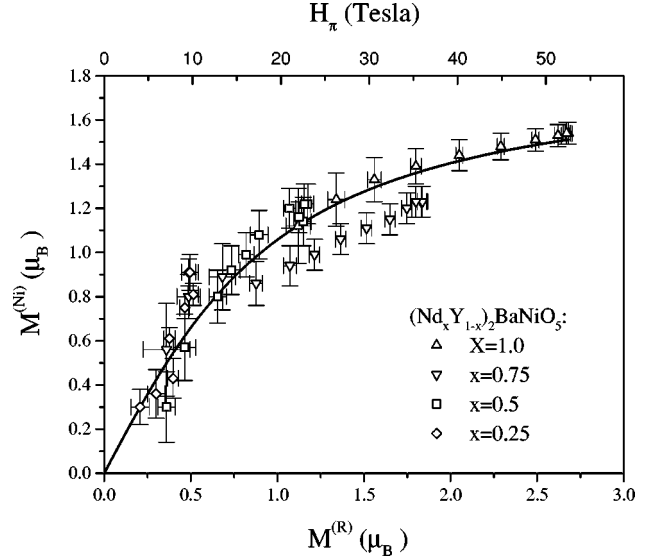


FIG. 13. Measured ordered Ni^{2+} moment in $(\text{Nd}_x\text{Y}_{1-x})_2\text{BaNiO}_5$ compounds plotted against the average ordered moment on the R sublattice (symbols, bottom axis). This dependence is interpreted as the staggered magnetization curve for an isolated Haldane spin chain. The estimated staggered exchange field acting on the Ni subsystem is shown on the top axis. The solid curve is an empirical fit to the experimental points, as described in Sec. IV [Eqs. (4)–(6)].

ordered moment is defined by the *intrinsic* temperature dependence of the susceptibility of individual chains. In contrast, in our case of $R_2\text{BaNiO}_5$ compounds, magnetic ordering is driven by the $1/T$ -divergent susceptibility of the rare-earth subsystem. At sufficiently low temperature long-range order will therefore occur for arbitrary small R-Ni interactions, and in the case of $T_N \leq \Delta$, we can use the approximation where the bare magnetization curve of isolated chains is T independent.

An important result of this work is that in *all samples studied* $m^{(\text{Ni})}$, the induced staggered moment on the Ni-chains, appears to be a universal function of $\tilde{m}^{(\text{Nd})} \equiv m^{(\text{Nd})}x$. In other words, the Ni magnetization explicitly depends only on the average moment on the R sites, and not the actual temperature, as illustrated in the plot of $m^{(\text{Ni})}$ vs $\tilde{m}^{(\text{Nd})}$ in Fig. 13. To emphasize the significance of this fact we reiterate that the ordering temperatures in the materials differ by more than a factor of 2. From Fig. 13 we see that even with fully ordered Nd^{3+} moments the Ni chains are not fully polarized and the curve never levels off completely. In the context of the HC/SF model, apart from the scaling of the absciss, Fig. 13 is nothing else but the *staggered magnetization function* $\mathcal{M}(H_\pi)$ for an isolated Haldane chain of Ni^{2+} spins, that in the studied temperature range $T=0-50$ K is expected to be almost T independent.

The role of disorder in Y-diluted systems is not too important, at least, in systems where the Nd concentration is not too small. The intrinsic dynamic spin correlation length of Haldane spin chains is rather large, of the order of six lattice repeats. As long as the mean distance between the Nd^{3+} ions is smaller than this length scale, the Ni chains effectively see a homogeneous staggered moment on the R sites, despite the ‘‘holes’’ that are present wherever Nd^{3+} is

replaced by Y^{3+} . The argument, while clearly valid at $T \approx T_N$, should be taken with some caution when applied to a system deep in the ordered phase. In this regime the Haldane-gap energy increases, and, as a consequence of that the dynamic correlation length in the chains decreases. Even in this case we can expect the effect of disorder to be averaged out, thanks to the simple geometrical fact that every Ni^{2+} ion is coordinated to four R sites.

We can now use the experimentally determined staggered magnetization function for Haldane spin chains in $(Nd_xY_{1-x})_2BaNiO_5$ to write down the self-consistent MF equations for our ‘‘semiquantum’’ theory. For the Ni-sublattice these equations are

$$m^{(Ni)} = gS\mu_B \mathcal{M}(H^{(Ni)}), \quad (4)$$

$$H^{(Ni)} = 2\alpha \tilde{m}^{(Nd)}. \quad (5)$$

Here $g\mu_B$ and $S=1$ are the gyromagnetic ratio and spin of Ni^{2+} , respectively; $H^{(Ni)}$ is the effective exchange field that acts on the Ni chains and is generated by the R sublattice; and α is an effective MF coupling constant. The factor 2 in Eq. (5) reflects the fact that there are two Nd atoms for every Ni atom in the chemical formula, while the magnetizations $m^{(Ni)}$ and $m^{(Nd)}$ are normalized per site. For convenience $\mathcal{M}(H^{(Ni)})$ in Eq. (4) is approximated with the following purely empirical function:

$$gS\mu_B \mathcal{M}(2\alpha \tilde{m}^{(Nd)}) = A \arctan(B\tilde{m}^{(Nd)}). \quad (6)$$

The coefficients $A=1.27(5)$ and $B=1.06(13)$ are obtained by fitting this formula to the bulk of experimental data in Fig. 13 (solid curves). To write down the remaining MF equations for the R sublattice we shall approximate the bare magnetization curve for the Nd^{3+} ions with the Brillouin function, as is appropriate for a magnetic ion with a doublet ground state:

$$m^{(Nd)} = m_0^{(Nd)} \tanh\left(\frac{m_0^{(Nd)} H^{(Nd)}}{\kappa T}\right). \quad (7)$$

$$H^{(Nd)} = \alpha m^{(Ni)}. \quad (8)$$

In this formula $H^{(Nd)}$ is the effective exchange field acting on the rare-earth ions, κ is Boltzmann’s constant, and $m_0^{(Nd)}$ is the effective magnetic moment for Nd^{3+} .

Ideally, the saturation moment m_0 should be independent of temperature or Nd concentration in the sample. In our particular systems, however, the saturation moment of the Nd^{3+} ions steadily decreases by roughly 25% as x changes from 1.0 to 0.25. Equation (7) is therefore no more than a crude approximation, and a 25% accuracy is the best we can expect from our model. Indeed, in using the Brillouin function to describe the rare earths, we have totally neglected the higher-energy electronic states of these ions. Not only do they contribute to the temperature dependence of R magnetization, but also may give rise to a T -independent Van Vleck contribution to single-ion susceptibility. Unfortunately, without knowing the electronic structure of R^{3+} in R_2BaNiO_5 in detail, we cannot take these effects into account rigorously.

Instead we shall use Eq. (7) with separate values for m_0 for each sample, equal to the saturation magnetization of the Nd sublattice.

Equations (4)–(8) were used to analyze the temperature dependences of sublattice magnetizations in three $(Nd_xY_{1-x})_2BaNiO_5$ samples, with $x=1$, $x=0.75$, and $x=0.5$. In the $x=0.25$ system the transition is of magnetoelastic nature, and a purely magnetic MF model cannot be expected to be applicable. For each sample composition the only adjustable parameter was the coupling constant α . The results of this analysis are shown in solid curves in Fig. 3. For the three samples we obtain $\alpha=0.84(2) \times 10^5 \text{ Oe } \mu_B^{-1}$, $\alpha=0.96(2) \times 10^5 \text{ Oe } \mu_B^{-1}$, and $\alpha=1.14(2) \times 10^5 \text{ Oe } \mu_B^{-1}$, respectively. As expected, for all three $(Nd_xY_{1-x})_2BaNiO_5$ systems the refined values of the coupling constant are very similar despite the substantially different ordering temperatures. We can use average value $\alpha=0.98(1) \times 10^5 \text{ Oe } \mu_B^{-1}$ to properly rescale the absciss in Fig. 13 and obtain the Ni order parameter as a function of effective exchange field, i.e., the actual *staggered magnetization curve for a Haldane spin chain* (Fig. 13, top axis). Differentiating Eq. (6) at $H^{(Ni)} \rightarrow 0$ we obtain the *staggered susceptibility* $\chi_\pi = 1.2 \times 10^{-5} \mu_B / \text{Oe}$.

The staggered magnetization curve for an isolated $S=1$ Heisenberg AF chain has not been calculated to date, and we cannot directly compare our results to any numerical simulations. The zero-temperature staggered susceptibility χ_π , on the other hand, can be deduced from the numerous theoretical predictions for the dynamic structure factor at the 1D AF zone center $S(\pi, \omega)$, to which it is related through the Kramers-Kronig relation and the fluctuation-dissipation theorem. In the single-mode approximation^{38,39,9} $S(\pi, \omega) = -\frac{4}{3} \langle \mathcal{H} \rangle / L \Delta \delta(\omega - \Delta)$. Here and $\langle \mathcal{H} \rangle / L$ is the ground-state energy per spin. According to Monte Carlo simulations (see, for example, Refs. 40,41), $\langle \mathcal{H} \rangle / L \approx -1.4J \approx 3.42\Delta$. The expression for the staggered susceptibility is then readily obtained via $\chi_\pi = 2 \int_0^\infty d\omega [S(\pi, \omega) / \omega]$ and is equal to

$$\chi_\pi = 9.1(g\mu_B)^2 / \Delta. \quad (9)$$

In all the R_2BaNiO_5 systems studied so far with inelastic neutron scattering the gap energies are equal to 9 meV to within experimental error, which gives $\chi_\pi \approx 2.3 \times 10^{-5} \mu_B / \text{Oe}$. This value is almost twice as large as our experimental estimate. While not spectacular, this level of consistency is quite acceptable, considering all the approximations and simplifications that had to be made. Most of the uncertainty is related to the large experimental error in the initial ‘‘low-field’’ part of the magnetization curve in Fig. 12 where small ordered moments were derived from the measurements in the vicinity of T_N , and the error bars are rather large. Some systematic error is introduced by approximating the measured curve with expression (6). We have also totally neglected the temperature dependence of the magnetization function for the Haldane spin chains, small as it may be at $\kappa T \lesssim 0.5\Delta$, and approximated that for the rare-earth ions by a simple Brillouin function. The actual gyromagnetic ratio for Ni^{2+} that enters Eq. (9) squared, is not known from independent measurements either. A half-order-of-magnitude agreement is indeed the most we can expect. What is important is that our model appears to be self-consistent and is based on

the same concepts as those previously used to explain the persistence and T dependence of Haldane-gap excitations in $R_2\text{BaNiO}_5$ materials.

B. The 4 meV mode

The excitation that we see at 4 meV energy transfer was observed in powder experiments,¹⁴ and attributed to a CF transition in Nd^{3+} . A similar feature was also seen in recent antiferromagnetic resonance measurements.⁴² As our single-crystal neutron data clearly demonstrate, the 4 meV mode has indeed no dispersion and its intensity is Brillouin-zone independent, so it indeed is a local, i.e., single-ion excitation(s). Despite that, we suggest that this mode *is* the actual order-parameter excitation (spin wave), and corresponds to flipping a single Nd^{3+} moment in the effective staggered field projected by the Ni sublattice. The energy of such an excitation is given by

$$\hbar\omega_0 = 2m_0H^{(\text{Nd})} = 2m_0\alpha m^{(\text{Ni})}. \quad (10)$$

The excitation energy should thus scale as the ordered moment of the Ni sublattice. The solid curve in Fig. 12 is drawn using Eq. (10), our experimental data for $m^{(\text{Ni})}(T)$ in $\text{Nd}_2\text{BaNiO}_5$, and $\alpha = 0.84 \times 10^5 \text{ Oe } \mu_B^{-1}$ determined from our MF analysis of the magnetic structure. An excellent agreement with inelastic measurements is apparent.

One possible explanation for the fully localized nature of the low-energy spin waves is a strong anisotropy in the effective exchange interaction between Ni^{2+} and Nd^{3+} . We suggest that this interaction is of Ising type, i.e., can be written as $J_{\text{eff}}^{\text{Ni}^2\text{Nd}^3} \mathbf{S}_{\text{Ni}^2, \text{eff}} \cdot \mathbf{S}_{\text{Nd}^3, \text{eff}}$ being the effective Nd spin. If one introduces this type of coupling between singlet ground state Ni-chains and isolated paramagnetic rare-earth ions at the RPA level, one obtains a total decoupling of the Ni- and Nd-transverse degrees of freedom. The Ni-chain modes are those of a Haldane system in a *static* staggered field. Those centered on Nd correspond to flipping a single paramagnetic moment, again in a *static* effective field. Interestingly, the low-energy excitations in $\text{Pr}_2\text{BaNiO}_5$ are qualitatively different: these are acoustic spin waves with a pronounced dispersion and structure factor.¹³ These excitations, as well as the higher-energy Haldane-gap modes, are expected to involve correlated fluctuations of both the Ni and the rare earth moments. The difference in behavior is, of course, due to the different electronic configuration of the rare-earth ions in $\text{Pr}_2\text{BaNiO}_5$ and $\text{Nd}_2\text{BaNiO}_5$ (Pr is not a Kramers ion and in $\text{Pr}_2\text{BaNiO}_5$ is, in fact, an induced-moment system), and the consequent difference in R -Ni magnetic interactions.

Unfortunately, within the MF model one cannot make any predictions regarding the strongly T -dependent damping of the 4 meV mode. Without going into further speculations, we would only like to point out that the measured magnitude and temperature dependence of γ is very similar to that of the temperature-induced broadening of Haldane-gap excitations, as measured in Y_2BaNiO_5 .²³ One possibility is that these quantities may actually be directly related and represent the same relaxation process.

C. Haldane-gap excitations in the Ni chains

Polarization

One set of results that we hoped to obtain from the inelastic thermal neutron-scattering experiments are separate temperature dependences of the Haldane-gap energies in each of the three components of the Haldane triplet. Of particular interest is the T dependence of the gap in the longitudinal mode, i.e., the one polarized along the ordered moments on the Ni sites. It has been predicted that the rate of increase of the longitudinal spin gap is three times larger than that of the two transverse gaps.¹⁸ As mentioned above, experimental difficulties make a complete polarization analysis impossible. At present, the only available results relevant to the multiplicity and polarization of Ni-chain gap excitations in $\text{Nd}_2\text{BaNiO}_5$ is the temperature dependence of integrated intensities measured at $\mathbf{Q}=(1.5,0,0)$ and $\mathbf{Q}=(0.5,0,4.2)$ (Fig. 8). To within experimental error these intensities are the same at all temperatures. At no instance do we see any distinct splitting in the energy gap. If we assume that the modes remain polarized along the principal crystallographic directions, as dictated by the local symmetry of the Ni sites, we are forced to conclude that the three components of the triplet evolve with temperature in exactly the same way.

The assumption however is expected to be valid only at $T \geq T_N$. As the magnetic order-induced shift in the Haldane-gap energies becomes larger than the initial anisotropy-induced splitting of the triplet (roughly 1 meV, according to Refs. 24,23), the proper choice of polarization axes is governed by the direction of the Ni^{2+} moments, rather than the crystallographic symmetry directions. In the magnetically ordered state the three excitations are polarized along the x' , y' , and z' axes, where y' runs along the $[010]$ direction, z' is chosen along the direction of ordered moments on the Ni sites and thus forms an angle of roughly 35° with the c axis of the crystal, and x' completes the orthogonal reper, respectively. The actual situation is even more complex, since two types of magnetic domains with the Ni^{2+} moments tilted to the left or to the right of the c -axis should be present in a macroscopic sample. As a result all three modes contribute to inelastic scattering at both $\mathbf{Q}=(1.5,0,0)$ and $\mathbf{Q}=(0.5,0,4.2)$, with partial intensities 0.33, 1, 0.67, and 0.63, 1, 0.37, correspondingly. We have concluded that our data are not inconsistent with seeing only the two transverse excitations (polarized along x' and z' , respectively). It is therefore entirely possible that for some reason we fail to see the longitudinal excitation altogether.

Definitive conclusions concerning the multiplicity and polarization of the gap excitations are premature. At this stage, however, we lean towards interpreting our data in terms of seeing only the transverse Haldane excitations in our scans. First of all, the longitudinal gap is expected to increase with decreasing T at least three times as fast as the transverse gaps. Below $T=40 \text{ K}$ it is expected to be already outside the range of our inelastic scans. Second, the observed temperature dependence of the Haldane-gap energies is in striking quantitative agreement with theoretical predictions for transverse modes (see next section). Third, it appears plausible that the appearance of an ordered moment on the Ni sites leads to the longitudinal mode being overdamped. Hopefully, the use of the very large sample B in future unpolarized and

polarized neutron-scattering experiments will help us resolve this issue.

D. Behavior of the Haldane-gap energy

As discussed in the previous section, our results for the low-energy spin waves indicate that magnetic excitations involving the Ni spins are totally decoupled from those in the Nd subsystem and are indistinguishable from transverse Haldane-gap excitations that occur in isolated Haldane chains in the presence of a *static* staggered field. The HC/SF model can thus be used in reference to spin dynamics, and not only the static magnetic properties of the system. Based on this assumption (that, at the time, was not backed by experimental results pertaining to the low-energy spin waves in the system), the increase of the Haldane-gap energy in the magnetically ordered state in $(\text{Nd}_x\text{Y}_{1-x})_2\text{BaNiO}_5$ was qualitatively explained in Ref. 18. In this work the staggered-field dependence of the Haldane-gap energies for a $S=1$ 1D Heisenberg antiferromagnet was derived through the use of a Ginsburg-Landau-like description of an isolated Haldane spin chain, the so-called ϕ^4 model, introduced in this context by Affleck.^{37,43}

In this approach an isolated Haldane spin chain is characterized by the space-dependent vector of local staggered magnetization $\vec{\phi}(x,t)$. The Lagrangian of the system is written as a series expansion in $\vec{\phi}(x)$ and its derivatives:

$$\mathcal{L} = \int dx \left[\frac{1}{2v} \left(\frac{\partial \vec{\phi}}{\partial t} \right)^2 - \frac{v}{2} \left(\frac{\partial \vec{\phi}}{\partial x} \right)^2 - \frac{\Delta^2}{2v} \vec{\phi}^2 - \lambda |\vec{\phi}|^4 + \text{higher-order terms} \right]. \quad (11)$$

The quadratic terms describe a triplet of degenerate noninteracting gap excitations (energy gap Δ) with a linear dispersion (spin-wave velocity v). A nonzero staggered-field dependence of the excitation energies appears upon introducing the $\lambda |\vec{\phi}|^4$ term, that represents pair repulsion between magnons, and other higher-order terms. In the presence of a staggered field, the change in gap energies, defined as $\delta(H_\pi) \equiv \{\Delta(H_\pi)^2 - \Delta_0^2\}/\Delta_0^2$, Δ_0 being the gap energy in the absence of any staggered field, for small fields is proportional to the square of the induced static staggered magnetic moment and the strength of magnon repulsion λ . In application to $R_2\text{BaNiO}_5$ systems, $\delta(H_\pi)$ is thus expected to scale proportionately to $[m^{(\text{Ni})}]^2$, as long as the ordered moment is small. This linear relation was confirmed for all previously studied $(\text{Nd}_x\text{Y}_{1-x})_2\text{BaNiO}_5$ systems.^{18,25}

The data obtained in the present work, particularly the more accurately measured temperature dependence of the Ni-sublattice magnetization, can be used to analyze the relation between Δ and $m^{(\text{Ni})}$ in greater detail. In order to do so, we first have to compensate for the intrinsic weak T dependence of the Haldane-gap energy. This is done by replacing Δ_0 by $\Delta_0(T)$, the temperature-dependent gap in the absence of staggered field. For $\Delta_0(T)$ we can take the Haldane gap measured as a function of temperature in Y_2BaNiO_5 , that, for practical purposes, we shall approximate by the following empirical formula:^{9,44}

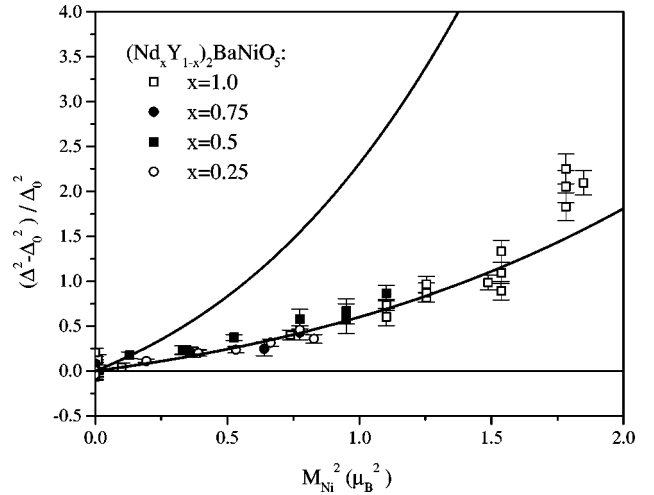


FIG. 14. Measured increase in the Haldane gap energy in $(\text{Nd}_x\text{Y}_{1-x})_2\text{BaNiO}_5$ compounds relative to that in Y_2BaNiO_5 plotted as a function of the square of the ordered staggered moment on the Ni chains (symbols). For $\text{Nd}_2\text{BaNiO}_5$ single-crystal data obtained in this work is shown. For the three other materials the data are taken from Ref. 15. The solid curves are theoretical predictions for the longitudinal and transverse gaps [Ref. 47 and Sec. IV, Eqs. (13),(14)].

$$\Delta_0(T) = \Delta_0(0) + \sqrt{\beta T} \exp(-\Delta_0(0)/\kappa T). \quad (12)$$

The coefficients $\Delta_0(0) = 9.21$ meV and $\beta = 1.0$ meV²/K were obtained by fitting this form to the experimental data for Y_2BaNiO_5 .^{22,23} This formula is used to plot $\delta(H_\pi)$ as a function of $[m^{(\text{Ni})}]^2$ for all four $(\text{Nd}_x\text{Y}_{1-x})_2\text{BaNiO}_5$ systems studied (Fig. 14). A perfect data collapse is obtained. Also apparent is the slow upward curvature of this function that could not be clearly seen when only powder data were available.¹⁸

In Ref. 18 no quantitative predictions regarding the slope of the linear relation between $\delta(H_\pi)$ and $[m^{(\text{Ni})}]^2$, i.e., the coefficient λ in Eq. (11), were made. Instead, λ was treated as an adjustable parameter. In a more refined approach λ is to be determined independently from the properties of the renormalization-group fixed point. This coefficient was recently calculated numerically.⁴⁵ The nonlinearity in the relation between $\delta(H_\pi)$ and $[m^{(\text{Ni})}]^2$ can be accounted for by including higher-order terms into the ϕ expansion of the Lagrangian. The corresponding coefficients, up to the eighth power in $\vec{\phi}$, were also recently computed.⁴⁶ These numerical results were then utilized to calculate the staggered-moment dependence of the gap energy for both transverse-polarized and longitudinal Haldane excitations:⁴⁷

$$\frac{\Delta_\perp^2 - \Delta_0^2}{\Delta_0^2} = 0.395(m^{(\text{Ni})})^2 + 0.156(m^{(\text{Ni})})^4 + 0.049(m^{(\text{Ni})})^6, \quad (13)$$

$$\frac{\Delta_\parallel^2 - \Delta_0^2}{\Delta_0^2} = 1.185(m^{(\text{Ni})})^2 + 0.78(m^{(\text{Ni})})^4 + 0.343(m^{(\text{Ni})})^6. \quad (14)$$

These equations have *no adjustable parameters* and for $\text{Nd}_2\text{BaNiO}_5$ systems yield the curves shown in solid curves

in Fig. 14. We see that our data almost perfectly agree with the prediction for the transverse-spin gap. The deviations at large $m^{(\text{Ni})}$ are expected, as the series in Eqs. (13),(14) are terminated at the third term. Assuming that what we observe in our experiments are transverse gap excitations, the HC/SF model thus gives *quantitatively correct* predictions for the temperature dependence of the gap energies.

V. CONCLUSION

The results of three independent series of experiments, powder neutron diffraction, and thermal- and cold-neutron inelastic scattering, are all consistent with our HC/SF model for $R_2\text{BaNiO}_5$ compounds at the quantitative level. The interactions between the Ni and rare-earth subsystems in $(\text{Nd}_x\text{Y}_{1-x})_2\text{BaNiO}_5$ can be to a very good approximation treated at the MF level. This description appears to apply very well not only to static magnetic properties, but also to

the spin dynamics. The dispersionless single-ion character of low-energy spin waves is a manifestation of an effective separation of the Ni-chain spin dynamics from that of the Nd subsystem.

ACKNOWLEDGMENTS

The authors would like to thank P. Convert, B. Malaman, J. L. Soubeyroux, and D. Neuman for their help with neutron-scattering experiments. This study was in part supported by the U.S.-Japan Cooperative Program on Neutron Scattering, a Grant-in-Aid for Scientific Research from the Ministry of Education, Science and Culture Japan and The Science Research Fund of Japan Private School Promotion Foundation. Work at Brookhaven National Laboratory was carried out under Contract No. DE-AC02-76CH00016, Division of Material Science, U.S. Department of Energy. Studies at NIST were partially supported by the NSF under Contract No. DMR-9413101.

-
- *Permanent address: Department of Physics, Aoyama-Gakuin University, 6-16-1, Chitosedai, Setagaya-ku, Tokyo 157 Japan.
- †Permanent address: DRFMC/SPSMS/MDN Center d'Etudes Nucleaires, 17 rue des Martyrs 38054 Grenoble Cedex, France.
- ‡Also at Department of Physics and Astronomy, Johns Hopkins University, MD 21218, and P. L. Kapitza Institute for Physical Problems, Moscow, Russia.
- ¹F. D. M. Haldane, *Phys. Rev. Lett.* **50**, 1153 (1983).
 - ²K. Kakurai, M. Steiner, R. Pynn, and J. K. Kjems, *J. Phys.: Condens. Matter* **3**, 715 (1991).
 - ³L. P. Regnault, C. Vettier, J. Rossat-Mignod, and J. P. Renard, *Physica B* **180-181**, 188 (1992).
 - ⁴T. Kobayashi *et al.*, *J. Phys. Soc. Jpn.* **63**, 1961 (1994).
 - ⁵L. P. Regnault and J. P. Renard, *Physica B* **243-236**, 541 (1997).
 - ⁶T. Sakai and M. Takahashi, *J. Phys. Soc. Jpn.* **62**, 750 (1993).
 - ⁷E. S. Sorensen and I. Affleck, *Phys. Rev. Lett.* **71**, 1633 (1993).
 - ⁸L. P. Regnault, I. Zaliznyak, J. P. Renard, and C. Vettier, *Phys. Rev. B* **50**, 9174 (1994).
 - ⁹S. Ma *et al.*, *Phys. Rev. Lett.* **69**, 3571 (1992).
 - ¹⁰M. Chiba *et al.*, *Phys. Rev. B* **44**, 2838 (1991).
 - ¹¹P. P. Mitra and B. I. Halperin, *Phys. Rev. Lett.* **72**, 912 (1994).
 - ¹²T. Sakai and H. Shiba, *J. Phys. Soc. Jpn.* **63**, 867 (1994).
 - ¹³A. Zheludev, J. M. Tranquada, T. Vogt, and D. J. Buttrey, *Europhys. Lett.* **35**, 385 (1996); *Phys. Rev. B* **54**, 6437 (1996).
 - ¹⁴A. Zheludev, J. M. Tranquada, T. Vogt, and D. J. Buttrey, *Phys. Rev. B* **54**, 7210 (1996).
 - ¹⁵T. Yokoo, Z. Zheludev, M. Nakamura, and J. Akimitsu, *Phys. Rev. B* **55**, 11 516 (1997).
 - ¹⁶J. Hernández-Velasco, R. Sáez-Puche, and J. Rodríguez-Carvajal, *Physica B* **234-236**, 569 (1997).
 - ¹⁷S. Raymond *et al.* (unpublished).
 - ¹⁸S. Maslov and A. Zheludev, *Phys. Rev. B* **57**, 68 (1998).
 - ¹⁹E. García-Matres, J. L. García-Munoz, J. L. Martínez, and J. Rodríguez-Carvajal, *J. Magn. Magn. Mater.* **149**, 363 (1995).
 - ²⁰J. Darriet and L. P. Regnault, *Solid State Commun.* **86**, 409 (1993).
 - ²¹J. F. DiTusa *et al.*, *Physica B* **194-196**, 181 (1994).
 - ²²T. Yokoo, T. Sakaguchi, K. Kakurai, and J. Akimitsu, *J. Phys. Soc. Jpn.* **64**, 3651 (1995).
 - ²³T. Sakaguchi, K. Kakurai, T. Yokoo, and J. Akimitsu, *J. Phys. Soc. Jpn.* **65**, 3025 (1996).
 - ²⁴G. Xu *et al.*, *Phys. Rev. B* **54**, 6827 (1996).
 - ²⁵A. Zheludev (unpublished); *Physica B* **241-243**, 495 (1998).
 - ²⁶V. Sachan, D. J. Buttrey, J. M. Tranquada, and G. Shirane, *Phys. Rev. B* **49**, 9658 (1994).
 - ²⁷A. Zheludev, J. P. Hill, and D. J. Buttrey, *Phys. Rev. B* **54**, 7216 (1996).
 - ²⁸E. García-Matres, J. L. Martínez, and J. Rodríguez-Carvajal, *Physica B* **234-236**, 567 (1997).
 - ²⁹A. Zheludev, E. Ressouche, S. Maslov, T. Yokoo, S. Raymond, and J. Akimitsu, *Phys. Rev. Lett.* **80**, 3630 (1998).
 - ³⁰E. García-Matres *et al.*, *J. Solid State Chem.* **103**, 322 (1993).
 - ³¹J. Rodríguez-Carvajal, *Physica B* **192**, 55 (1993).
 - ³²L. Koester, H. Rauch, and E. Seymann, *At. Data Nucl. Data Tables* **49**, 65 (1991).
 - ³³P. J. Brown, in *International Tables for Crystallography*, edited by A. J. C. Wilson (Kluwer, Dordrecht, 1992), pp. 391–399.
 - ³⁴E. García-Matres, J. Rodríguez-Carvajal, J. L. Martínez, and A. Salinas-Sánchez, *Solid State Commun.* **85**, 553 (1993).
 - ³⁵D. J. Scalapino, Y. Imry, and P. Pincus, *Phys. Rev. B* **11**, 2042 (1975).
 - ³⁶W. J. L. Buyers *et al.*, *Phys. Rev. Lett.* **56**, 371 (1986); R. M. Morra *et al.*, *Phys. Rev. B* **38**, 543 (1988), and references therein.
 - ³⁷I. Affleck, *Phys. Rev. Lett.* **62**, 474 (1989).
 - ³⁸D. P. Arovos, A. Auerbach, and F. D. M. Haldane, *Phys. Rev. Lett.* **60**, 531 (1988).
 - ³⁹G. Muller, H. Thomas, M. W. Puga, and H. Beck, *J. Phys. C* **14**, 3399 (1981).
 - ⁴⁰S. Liang, *Phys. Rev. Lett.* **64**, 1597 (1990).
 - ⁴¹S. V. Meshkov, *Phys. Rev. B* **48**, 6167 (1993).
 - ⁴²S. Okubo, H. Ohta, M. Hayashi, H. Kikuchi, M. Motokawa, and H. Nagasawa (unpublished).
 - ⁴³I. Affleck and G. F. Wellstein, *Phys. Rev. B* **46**, 8934 (1992).
 - ⁴⁴A. Zheludev *et al.*, *Phys. Rev. B* **53**, 15 004 (1996).
 - ⁴⁵A. Pelissetto and E. Vicari, *Nucl. Phys. B* **519**, 626 (1998).
 - ⁴⁶A. Pelissetto and E. Vicari, *Nucl. Phys. B* **522**, 605 (1998).
 - ⁴⁷S. Maslov and A. Zheludev, *Phys. Rev. Lett.* **80**, 5786 (1998).